

Non-Fermi liquid behavior with and without quantum criticality in $\text{Ce}_{1-x}\text{Yb}_x\text{CoIn}_5$

T. Hu,^{1,*} Y. P. Singh,^{1,*} L. Shu,² M. Janoschek,² M. Dzero,¹ M. B. Maple,² and C. C. Almasan,¹

¹*Department of Physics, Kent State University, Kent, OH 44242, USA*

²*Department of Physics, University of California at San Diego, La Jolla, CA 92003, USA*

(Dated: August 23, 2012)

PACS numbers: 71.10.Hf, 71.27.+a, 74.70.Tx

One of the greatest challenges to Landau's Fermi liquid theory - the standard theory of metals - is presented by complex materials with strong electronic correlations. In these materials, non-Fermi liquid transport and thermodynamic properties are often explained by the presence of a continuous quantum phase transition which happens at a quantum critical point (QCP). A QCP can be revealed by applying pressure, magnetic field, or changing the chemical composition. In the heavy-fermion compound CeCoIn_5 , the QCP is assumed to play a decisive role in defining the microscopic structure of both normal and superconducting states. However, the question of whether QCP must be present in the material's phase diagram to induce non-Fermi liquid behavior and trigger superconductivity remains open. Here we show that the full suppression of the field-induced QCP in CeCoIn_5 by doping with Yb has surprisingly little impact on both unconventional superconductivity and non-Fermi liquid behavior. This implies that the non-Fermi liquid metallic behavior could be a new state of matter in its own right rather than a consequence of the underlying quantum phase transition.

The heavy-fermion material CeCoIn_5 is a prototypical system in which strong interactions between conduction and predominantly localized f -electrons give rise to a number of remarkable physical phenomena [1, 2]. Unconventional superconductivity emerges in CeCoIn_5 out of a metallic state with non-Fermi-liquid (NFL) properties: linear temperature dependence of resistivity below 20 K, logarithmic temperature dependence of the Sommerfeld coefficient, and divergence of low temperature magnetic susceptibility [3–6]. These anomalies disappear beyond a critical value of the magnetic field and the system recovers its Fermi liquid properties. The crossover from non-Fermi liquid to Fermi liquid behavior is thought to be governed by a quantum critical point (QCP), which separates paramagnetic and antiferromagnetic (AFM) phases and is located in the superconducting phase [7, 8]. Neutron scattering studies [9] and more recent measurements of the vortex-core dissipation through current-voltage characteristics [10] provide direct evidence for an antiferromagnetic QCP in CeCoIn_5 that could be accessed by tuning the system via magnetic field or pressure.

Nevertheless, a growing number of f -electron systems do not conform with this QCP scenario; for example, the NFL behavior in some systems occurs in the absence of an obvious QCP [11, 12]. An intriguing candidate is Yb-doped CeCoIn_5 that exhibits an unconventional $T - x$ phase diagram without an apparent QCP, while the onset of coherence in the Kondo lattice and the superconducting transition temperature T_c are only weakly dependent on Yb concentration and prevail for doping up to $x = 0.65$. [13]. Yet, the presence of a QCP in the parent CeCoIn_5 compound and the logarithmic temperature dependence of normal state Sommerfeld coefficient in lightly doped $\text{Ce}_{1-x}\text{Yb}_x\text{CoIn}_5$ crystals [14] show that this system is in the vicinity to a QCP. Therefore, it is important to elucidate the nature of the NFL behavior and unconventional superconductivity in such a system, to search for possible QCPs, and to determine the degree to which quantum criticality and superconductivity are coupled to each other.

Here we focus on revealing a field-induced quantum critical point through normal-state magnetoresistivity measurements and finding its evolution with Yb-doping. Experimental details are given in the "Materials and Methods" Section. We first present the results of our study of the magnetic field H and temperature dependence of the transverse ($H \perp ab$) in-plane magnetoresistivity $\Delta\rho_a^\perp/\rho_a \equiv [\rho_a^\perp(H) - \rho_a(0)]/\rho_a(0)$, for $H \leq 14$ T and $3 \leq T \leq 70$ K. Figure 1(a) and its inset display the field dependence of $\Delta\rho_a^\perp/\rho_a$ measured at different temperatures for the $x = 0$ and $x = 0.4$ samples, respectively. We note that the data for these samples fall into two groups: (i) non-monotonic field dependence of magnetoresistivity (MR) [Fig. 1(a)] with quadratic MR at high fields, typical for $x \leq 0.20$ and (ii) negative and quadratic MR over the whole measured field range [inset to Fig. 1(a)], typical behavior for the high Yb ($0.25 \leq x \leq 0.65$). We, therefore, conclude that the MR for low Yb doping has two main contributions: one negative and quadratic in H , which we denote $\Delta\rho_a^{\text{orb}}/\rho_a$ [black symbols of Fig. 1(b) at high fields] and the other is *positive* denoted $\Delta\rho_a^{\text{spin}}/\rho_a$ [green symbols of Fig. 1(b)], with the latter one obtained by subtracting for all field values the negative quadratic MR from the measured MR. This latter contribution to MR is isotropic since the green data follow quite well the longitudinal magnetoresistivity $\Delta\rho_a^\parallel/\rho_a$ [red data of Fig. 1(b)]. Also, $\Delta\rho_a^{\text{spin}}/\rho_a$ is linear

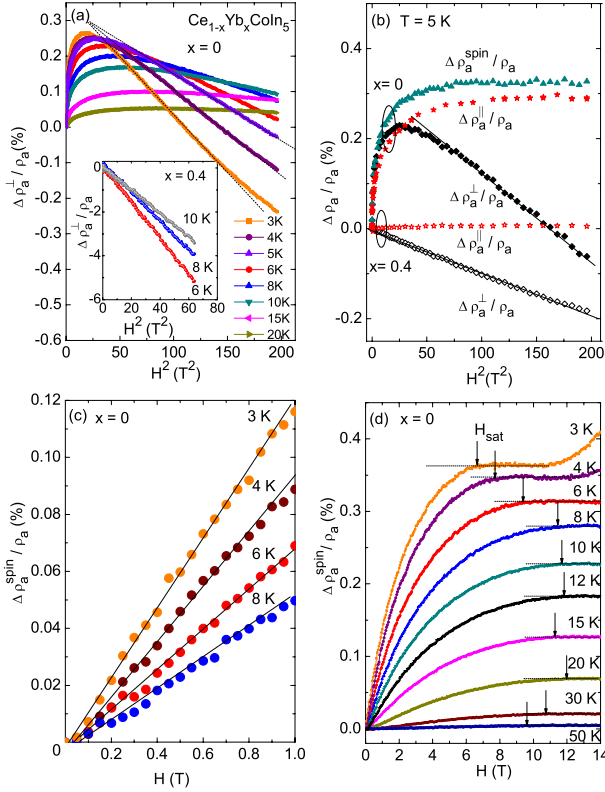


FIG. 1: (Color online) (a) Magnetic field H scans of transverse magnetoresistivity $\Delta\rho_a^\perp/\rho_a$ measured at different temperatures on $\text{Ce}_{1-x}\text{Yb}_x\text{CoIn}_5$ for $x = 0$ (main panel) and $x = 0.4$ (inset). (b) In-plane transverse $\Delta\rho_a^\perp/\rho_a$ (black) and longitudinal $\Delta\rho_a^\parallel/\rho_a$ (red) magnetoresistivities (MR) of $x = 0$ and $x = 0.4$ samples vs H^2 measured at 5 K. The green data are denoted $\Delta\rho_a^{\text{spin}}/\rho_a$ and represent the component of MR obtained by subtracting the high field quadratic MR from the measured transverse MR. (c) $\Delta\rho_a^{\text{spin}}/\rho_a$ vs H (for low H values) for the $x = 0$ sample measured at different temperatures. (d) H dependence of the isotropic component $\Delta\rho_a^{\text{spin}}/\rho_a$ of transverse magnetoresistivity of CeCoIn_5 measured at different temperatures and up to 14 T.

in H at low fields [Fig. 1(c)] and saturates at high fields [Fig. 1(d)].

Positive MR of heavy-fermion materials at low fields marks the departure from the single-ion Kondo behavior and is determined by the formation of the coherent Kondo lattice state in systems in or close to their Fermi-liquid ground state [15–20]. The maximum in the MR of a Kondo-lattice Fermi liquid at a certain field value is a result of the competition between a T -independent residual resistivity contribution that increases with increasing H , and a T -dependent term that decreases with increasing H [20, 21]. Thus, in conventional Kondo lattice systems, the peak in the field-dependent MR moves toward lower H with increasing T since a lower field is required to break the Kondo lattice coherence.

To determine the nature of the positive magnetoresistance in $\text{Ce}_{1-x}\text{Yb}_x\text{CoIn}_5$ for $x \leq 0.20$, we extract

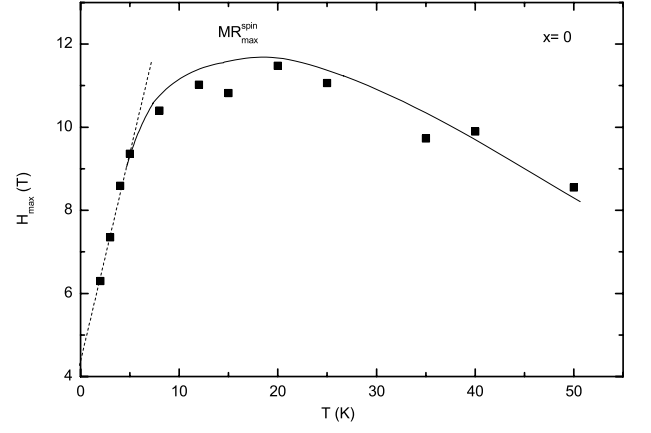


FIG. 2: Temperature dependence of the characteristic field H_{max} corresponding to the maximum isotropic component of magnetoresistance $MR_{\text{max}}^{\text{spin}}$. The solid line is a guide to the eye, while the dotted line is a linear fit of the low- T linear behavior of H_{max} for the $x = 0$ sample.

the temperature dependence of the field H_{max} at which $\Delta\rho_a^{\text{spin}}/\rho_a$ saturates at its maximum value $MR_{\text{max}}^{\text{spin}}$ [see Fig. 1(d)]. The data of Fig. 2 show that the temperature dependence of H_{max} of the $x = 0$ sample is non-monotonic, with a maximum around 20 K, and a linear behavior at low- T values. This non-monotonic T behavior of H_{max} is representative for all the samples with $x \leq 0.20$. The positive MR measured at $T > 20$ K [for which $H_{\text{max}}(T)$ decreases with increasing T] could reflect the presence of the coherent Kondo lattice state at low field values as discussed in the previous paragraph. In contrast, the behavior below 20 K is opposite with the one discussed above for conventional Kondo lattice systems. The increase of H_{max} with increasing T at these lower temperatures had previously been observed in CeCoIn_5 and it has been attributed to field quenching of the AFM spin fluctuations responsible for the NFL behavior [22]. Therefore, we conclude that the positive MR measured at $T < 20$ K in $\text{Ce}_{1-x}\text{Yb}_x\text{CoIn}_5$ with $x \leq 0.20$ reflects the dominant role played by the AFM quantum spin fluctuations.

An important next goal is to identify the quantum critical field (H_{QCP}) associated with these quantum fluctuations. One option is to extrapolate the low temperature linear $H_{\text{max}}(T)$ behavior to $T = 0$ K and identify this $H_{\text{max}}(0)$ with H_{QCP} . However, since there is a certain error associated with the determination of H_{max} , we adopted a more accurate procedure to unambiguously determine H_{QCP} for different Yb doping. This procedure is discussed in detail in the “Materials and Methods” Section below. We show in Fig. 3(a) the values of H_{QCP} as a function of Yb concentration. As expected, the value of H_{QCP} of 4.1 T for CeCoIn_5 coincides with the value of H_{QCP} determined previously from both resistivity measurements done in the normal state [23] and $I - V$ char-

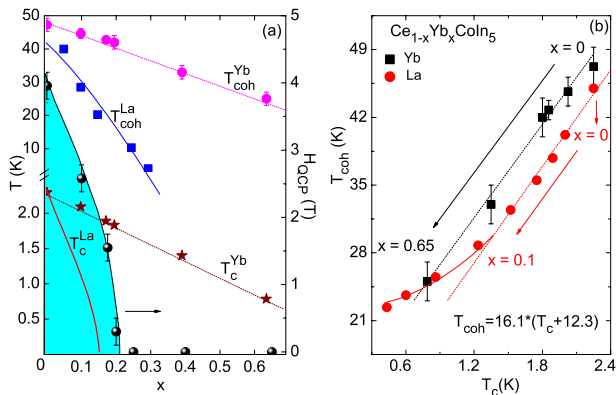


FIG. 3: (Color online) (a): Evolution of the field induced quantum critical point H_{QCP} , coherence temperature T_{coh} , superconducting critical temperature T_c (from Ref. [13]) of $Ce_{1-x}R_xCoIn_5$ ($R = Yb, La$) as a function of rare-earth concentration x . (b): Plot of T_{coh} vs. T_c for Yb- and La-doped (from Ref. [3]) samples.

acteristics measured in the mixed state [10]. Therefore, the measurement of $\Delta\rho_a^\perp/\rho_a$ along with the analysis used here represent an excellent experimental technique to determine the field-induced QCP in the NFL regime. The $H_{QCP} = 0$ points in Fig. 3(a) for $x > 0.20$ correspond to the case when there is no positive MR, i.e., the maximum in MR shifts to zero field [see inset to Fig. 1(a)].

Figure 3(a) also shows the suppression of T_c (from [13]) and T_{coh} with doping for $Ce_{1-x}Yb_xCoIn_5$. These doping-dependent H_{QCP} and temperature phase diagrams show that while superconductivity (SC) is robust and survives over the whole Yb doping range, the field-induced QCP is strongly suppressed with Yb doping and disappears for $x > 0.20$. This implies that SC and quantum criticality are likely to be decoupled in this system, i.e., unconventional superconductivity is not triggered by spin fluctuations.

The experimental technique used to determine H_{QCP} also permits the determination of the gyromagnetic factor g (see "Materials and Methods" Section below). There is a significant change in the value of the g factor at QCP, from 2.2 just below H_{QCP} to 1.3 just above H_{QCP} . This means that for $H < H_{QCP}$ the conduction electrons become weakly coupled to the local spins, so that the heavy-fermions would have a lower effective mass. However, for $H > H_{QCP}$ the antiferromagnetic fluctuations between the local moments are suppressed, so that the heavy-fermions recover their effective mass and this is reflected in the reduction in the value of the g -factor [25].

Figure 3(b) shows that T_{coh} (from this work) scales with T_c (from Ref. [13]) over the whole Yb doping studied here ($x \leq 0.65$) (black squares) and La doping (red circles, data from Ref. [3]). We note that T_{coh} vs T_c follows a linear dependence for the whole Yb doping with $x \leq 0.65$ and up to about 10% La doping, with the two

slopes having about the same value; this figure also shows the result of the linear fit for the Yb doping. Thus, it is intriguing that while the scaling of these two temperatures is in conformity to the other rare-earth substitutions on the Ce site [24], the nature of the scaling sets the Yb substitution aside from the other rare-earth substitutions since, in the latter ones a non linear and quite fast suppression of both temperatures is observed, with a suppression of T_c to zero at around $x = 17.6\%$ of rare-earth substitution (see Fig. 3(a), data from [3, 13]).

A very interesting and puzzling behavior of the $Ce_{1-x}Yb_xCoIn_5$ system is that, even though QCP disappears for $x > 0.20$, the system continues to display NFL behavior, as evidenced by the sublinear T -dependence of its resistivity [13]. This means that this non-Fermi liquid behavior at higher Yb doping could be a new state of matter in its own right rather than a consequence of the underlying quantum phase transition. We further investigated the origin of this NFL behavior by studying in more detail the T dependence of the resistivity measured in different magnetic fields. The resistivity of all the Yb-doped single crystals studied follow remarkably well the expression $\rho_a^\perp(H) = \rho_0 + AT + B\sqrt{T}$ for temperatures up to about 15 K [see inset to Fig. 4(a) for the fitting results] and in fields up to 14 T; here ρ_0 , A , and B are doping- and field-dependent fitting parameters. We show in Figs. 4(a) and 4(b) the doping and magnetic field dependences, respectively, of the ratio of the T -linear contribution to the total T -dependent contribution of the resistivity. These results show that the linear in T term in resistivity is present for low Yb doping ($x \leq 0.20$) in the quantum critical regime ($T \leq 20$ K). The percentage of the linear in T term decreases with increasing x and H and disappears for $x > 0.20$ and at fields at which the MR is only negative, where only the \sqrt{T} dependence is present. The bottom inset to Fig. 4(a) shows the average Yb valence as a function of Yb doping [26]. It is noteworthy that the average Yb valence decreases with increasing Yb and saturates to a value of about 2.3 for $x > 0.20$ [26, 27]. This result along with the data of Figs. 4(a) and 4(b) and the fact that both the superconducting transition and coherence temperatures remain weakly dependent on doping indicate that Yb atoms form a co-operative mixed-valence state that significantly reduces the pair-breaking effects, which could also play an important role in the origin of the NFL behavior at these higher Yb concentrations ($x > 0.20$). This idea is supported by the observed linear dependence of T_{coh} vs T_c [Fig. 3(b)]. The "Materials and Methods" Section gives more discussion and interpretation of this scaling.

All of the above observations show that the field-induced QCP plays a supporting rather than competing role in the emergence of unconventional superconductivity. Moreover, we conclude that a highly unusual microscopic mechanism of unconventional superconductivity in $Ce_{1-x}Yb_xCoIn_5$ may be at play: on one hand, the

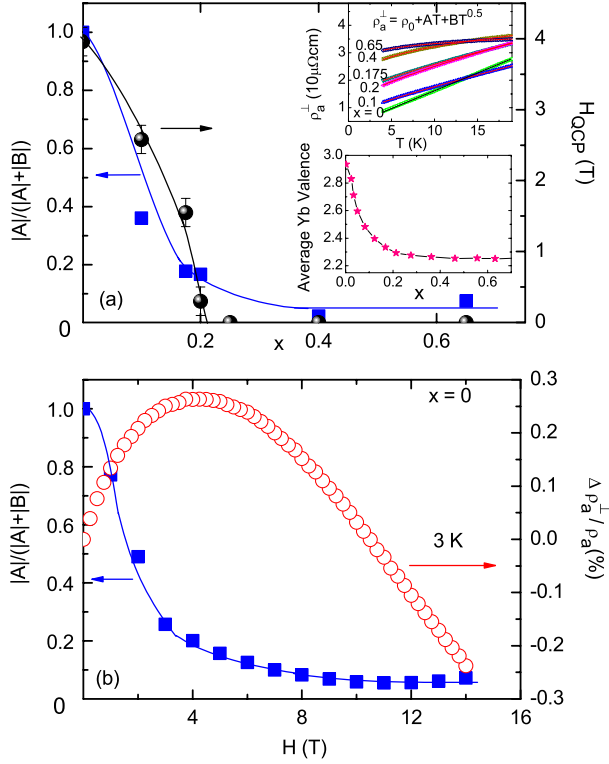


FIG. 4: (color online) (a) Doping dependence of linear in temperature T contribution divided by the total contribution to the resistivity obtained from fits (shown in the top inset) of the resistivity data by $\rho_a^\perp(H) = \rho_0 + AT + B\sqrt{T}$, along with the evolution of the field-induced QCP $H_{QCP}(x)$ (main panel). Bottom inset: Variation of average Yb valence with doping (data from Ref. [26]). (b) Field dependence of the linear in T contribution over the total contribution to the resistivity (left axis) and magnetoresistivity (right axis) measured at 3 K for pure CeCoIn_5 .

normal state is fully reconstructed by the ytterbium substitution, while on the other hand, the superconducting critical temperature is reduced only by a factor of two at $x \simeq 65\%$, strongly suggesting that the superconducting pairing is spatially inhomogeneous and involves local Ce f -moments. Finally, we propose a novel technique to probe the interplay between quantum criticality and superconductivity, which can be used to analyze a variety of strongly correlated electronic materials.

MATERIALS AND METHODS

In this Section we provide the supplementary discussion for the background material that will enable one to reproduce our results. First, we outline how the samples were prepared and describe the experimental methods used to determine the magnetoresistance and its dependence on magnetic field and temperature. Then, we show how describe the procedure we developed to determine

the field-induced quantum critical point from magnetoresistivity data. Finally, we offer an interpretation of the scaling of the Kondo lattice coherence temperature and superconducting critical temperature.

Experimental methods

Single crystals of $\text{Ce}_{1-x}\text{Yb}_x\text{CoIn}_5$ ($0 \leq x \leq 0.70$) were grown using an indium self-flux method [28]. The crystal structure and composition were determined from X-ray powder diffraction (XRD) and energy dispersive X-ray (EDX) techniques. The single crystals have a typical size of $2.1 \times 1.0 \times 0.16 \text{ mm}^3$, with the c axis along the shortest dimension of the crystals. They were etched in concentrated HCl for several hours to remove the indium left on the surface during the growth process and were then rinsed thoroughly in ethanol. Four leads were attached to the single crystal, with $I \parallel a$. High quality crystals were chosen to perform in-plane transverse ($\Delta\rho_a^\perp/\rho_a$) and longitudinal ($\Delta\rho_a^\parallel/\rho_a$) magneto-resistivity (MR) measurements, with $H \perp ab$ and $H \parallel ab$, respectively, as a function of temperature (T) and applied magnetic field (H). In both situations, however, the field is perpendicular to the current, $\vec{H} \perp \vec{I}$, to ensure that Lorentz force remains the same.

Determination of field-induced quantum critical point

We used the following procedure to determine the quantum critical field H_{QCP} for different Yb doping. We define the characteristic fields H_{max} where $\Delta\rho_a^{spin}/\rho_a$ is 100%, 95%, 80%, 75%, etc. of the saturation value MR_{max}^{spin} . We show the T dependence of these characteristic fields in Fig. 5(a) by the black, red, green, and blue solid circles, respectively. We then fit the linear low- T behavior of these $H_{max}(T)$. Figure 5(b) is a plot of the slopes K (black solid circles), obtained from these linear fits of the different curves with different percentages of MR_{max}^{spin} [Fig. 5(a)], and the corresponding percentage of MR_{max}^{spin} (red solid squares) vs the corresponding values of the intercept fields $H_{max}(0)$. We note the sharp increase of the slope K , at a certain $H_{max}(0)$ value.

g-factor and Kondo breakdown

The origin of the sharp increase in the values of K can be interpreted as follows. For a system in the quantum critical regime [i.e., low H and T data of Fig. 5(a)], the only energy scale is Boltzmann energy $\mathcal{E}_T = k_B T$. We compare this energy scale \mathcal{E}_T to the quasiparticle Zeeman energy, i.e.,

$$k_B T = g\mu_B(H - H_{QCP}). \quad (1)$$

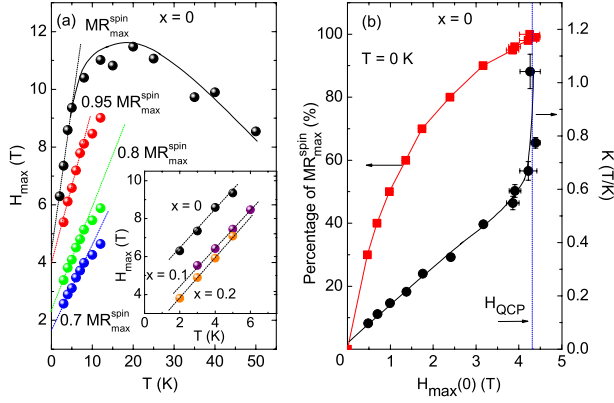


FIG. 5: (Color online) (a): Temperature dependence of the characteristic field H_{max} determined for different percentages of the maximum isotropic component of magnetoresistance MR_{max}^{spin} (main panel) and low- T linear behavior of H_{max} for $0 \leq x \leq 0.20$ samples (inset) (b): Slopes K (black solid circles) and percentage of MR_{max}^{spin} as a function of the corresponding values of the intercept fields $H_{max}(0)$.

From Eq. (1) we see that the slope K [Fig. 5(a)] must be inverse proportional to the gyromagnetic factor g . So, the sharp increase in K is a result of the sharp decrease in g . Previous studies [29] have shown that abrupt changes in the values of the gyromagnetic factor occur at the quantum critical point. Therefore, using this procedure we are able to unambiguously determine H_{QCP} as the value of $H_{max}(0)$ at which there is the sharp change in the g factor. Specifically, we find that g decreases from 2.2 just below H_{QCP} to 1.3 just above H_{QCP} .

The experimentally observed changes in the g -factor reflect the transformations that the electronic system undergoes under the change in external magnetic field. Given that $g \simeq 2.2$ just below H_{QCP} , numerically close to the value found for the free electrons in a metal, suggests that the conduction electrons become decoupled from the local f -moments below the QCP. Thus, this observation can be interpreted using the phenomenological theory of "Kondo breakdown" at H_{QCP} [30]. Within this theory, the changes in the g -factor are governed by the changes in the size of the Fermi surface: larger values of the g -factor correspond to small Fermi surface so that the conduction electrons are effectively decoupled from the localized f -states. In the opposite limit of smaller g -values, the Fermi surface is large, reflecting the strong coupling between the conduction and f -electrons. More importantly, the jump in the size of the Fermi surface at H_{QCP} corresponds to the divergence of the quasiparticle's effective mass.

SCALING OF THE COHERENCE TEMPERATURE

In this Section, we discuss and offer an interpretation of our data for the concentration dependence of the Kondo lattice coherence temperature (T_{coh}) and superconducting critical temperature (T_c). For definiteness, we focus primarily on the concentration region $x \leq 0.5$, where T_{coh} can be interpreted as a heavy-fermion coherence temperature of the Ce f -moments.

We start with the following observation: by combining our results on the concentration dependence of the coherence temperature and the critical temperature of the superconducting transition, we find that to a good accuracy both of them are suppressed at the same rate, i.e.,

$$T_{coh}^{Yb}(x) = \alpha_{Yb} T_c^{Yb}(x) + \beta_{Yb}, \quad (2)$$

where

$$\alpha_{Yb} = 16.1 \pm 0.2, \quad \beta_{Yb} = 4.09 T_{coh}(x=0). \quad (3)$$

To get better insight into the physical meaning of this result, it is instructive to compare Eq. (2) with the same dependence obtained for La-substituted CeCoIn₅. We find that in this case T_{coh} also scales with T_c at small enough concentration of La [Fig. 2(b) in the main text]:

$$T_{coh}^{La}(x) = \alpha_{La} T_c^{La}(x) + \beta_{La}. \quad (4)$$

The slight offset between the two curves, Fig. 2(b), appears likely because of atomic size differences between Yb and La ions. What is truly surprising is that the rate at which both T_{coh} and T_c are suppressed turns out to be the same for both types of substitutions:

$$\alpha_{Yb} \simeq \alpha_{La}. \quad (5)$$

We interpret Eq. (5) as an indication that the onset of the many-body coherence in the Kondo lattice and emergence of superconductivity has the same physical origin: hybridization between conduction and localized f -electron states. In particular, this suggests that Cooper pairing develops primarily on the "heavy" (i.e., large) Fermi surface.

Note that, although the suppression rate of Kondo lattice coherence and superconductivity for both Yb- and La-substitutions are the same, both T_{coh}^{Yb} and T_c^{Yb} remain much more robust with respect to disorder. This fact can be explained by noting that Yb atoms are in a mixed valence state and, therefore, must be correlated. The correlation may arise via local lattice deformations. To see how the impurity correlations may slow down the suppression of the coherence temperature, we may consider the characteristic length scale R on which impurity distribution function significantly deviates from unity. The

impurity distribution function determines the probability with which one can find one impurity at a certain distance from another. Within the Born approximation, one can show that there will be two contributions to the self-energy of the conduction electrons. One contribution, Σ_{ii} , corresponds to the scattering of electrons on the same impurity and, upon the averaging over disorder, this contribution is proportional to the concentration of impurities n_{imp} . The second contribution, Σ_{ij} , describes the scattering of electrons on two different impurities and, therefore, is proportional to n_{imp}^2 . In the presence of impurity correlations, however, Σ_{ij} becomes proportional to $n_{imp}^2 R^3$. Thus, if the radius of correlations is large enough, $n_{imp} R^3 \sim 1$, Σ_{ij} becomes comparable with the first, linear in n_{imp} , self-energy correction Σ_{ii} . Consequently, within the large- N mean field theory, one can show that impurity correlations may provide the "healing effect": the rate of suppression of the coherence temperature becomes strongly dependent on the impurity correlation length, R [31].

ACKNOWLEDGEMENTS

This work was supported by the National Science Foundation (grant NSF DMR-1006606 and DMR-0844115), ICAM Branches Cost Sharing Fund from Institute for Complex Adaptive Matter, and Ohio Board of Regents (grant OBR-RIP-220573) at KSU, and by the U.S. Department of Energy (grant DE-FG02-04ER46105) at UCSD. MJ gratefully acknowledges financial support by the Alexander von Humboldt foundation.

* These authors had equal contribution.

-
- [1] P. Coleman. Heavy fermions: electrons at the edge of magnetism, *Handbook of Magnetism and Advanced Magnetic Materials*, Vol 1, 95-148 (Wiley, 2007).
 - [2] J. L. Sarrao and J. D. Thompson. Superconductivity in cerium- and plutonium-based '115' materials. *Jour. of Phys. Soc. Japan* **76**, 051013 (2007).
 - [3] S. Nakatsuji, S. Yeo, L. Balicas, Z. Fisk, P. Schlottmann, P. G. Pagliuso, N. O. Moreno, J. L. Sarrao, and J. D. Thompson. Intersite coupling effects in a Kondo lattice. *Phys. Rev. Lett.* **89**, 106402 (2002).
 - [4] C. Petrovic, P. G. Pagliuso, M. F. Hundley, R. Movshovich, J. L. Sarrao, J. D. Thompson, Z. Fisk, and P. Monthoux. Heavy-fermion superconductivity in CeCoIn₅ at 2.3 K. *J. Phys. Condens. Matter* **13**, L337L342 (2001).
 - [5] R. Movshovich, *et al.* Unconventional superconductivity in CeIrIn₅ and CeCoIn₅: specific heat and thermal conductivity studies. *Phys. Rev. Lett.* **86**, 5152-5155 (2001).
 - [6] J. S. Kim, J. Alwood, G. R. Stewart, J. L. Sarrao and J. D. Thompson. Specific heat in high magnetic fields and non-Fermi-liquid behavior in CeMIn₅ (M = Ir, Co). *Phys. Rev. B* **64**, 134524 (2001).
 - [7] J. Paglione *et al.* Field-Induced Quantum Critical Point in CeCoIn₅. *Phys. Rev. Lett.* **91**, 246405 (2003).
 - [8] S. Singh *et al.* Probing the Quantum Critical Behavior of CeCoIn₅ via Hall Effect Measurements. *Phys. Rev. Lett.* **98**, 057001 (2007).
 - [9] M. Kenzelmann *et al.* Coupled superconducting and magnetic order in CeCoIn₅. *Science* **321**, 1652 (2008).
 - [10] T. Hu, H. Xiao, T.A. Sayles, M. Dzero, M.B. Maple, C.C. Almasan. Strong magnetic fluctuations in superconducting state of CeCoIn₅. *Phys. Rev. Lett.* **108**, 056401 (2012).
 - [11] Y. Matsumoto *et al.* Quantum criticality without tuning in the mixed valence compound β -YbAlB₄. *Science* **331**, 316-319 (2011).
 - [12] M. B. Maple, R. E. Baumbach, N. P. Butch, J. Hamlin, M. Janoschek. Non-Fermi liquid regimes and superconductivity in the low temperature phase diagrams of strongly correlated d - and f -electron materials. *J. Low Temp. Phys.* **161**, 4-54 (2010).
 - [13] L. Shu *et al.* Correlated electron state in Ce_{1-x}Yb_xCoIn₅ stabilized by cooperative valence fluctuations. *Phys. Rev. Lett.* **106**, 156403 (2011).
 - [14] E. D. Bauer *et al.* Electronic inhomogeneity in a Kondo lattice. *Proc. Natl. Acad. Sci.* **108**, 6857-6861 (2011).
 - [15] P. T. Coleridge. Magnetoresistance and growth of the coherent state in CeCu₆. *J. Phys. F: Met. Phys.* **17**, L79-85 (1987).
 - [16] J. Ruvalds and Q. G. Sheng. Magnetoresistance in heavy-fermion alloys. *Phys. Rev. B* **37**, 1959-1968 (1988).
 - [17] J. Flouquet, P. Haen, F. Lapierre, C. Fierz, A. Amato, and D. Jaccard. Residual resistivity in cerium heavy fermion compounds. *J. Magn. Magn. Mater.* **76-77**, 285-286 (1988).
 - [18] U. Rauchschwalbe, F. Steglich, A. de Visser and J. J. M. Franse. Magnetoresistance of Ce-based Kondo lattices: CeCu₂Si₂ and CeAl₃. *J. Magn. Magn. Mater.* **63-64**, 347-348 (1987).
 - [19] M. C. Aronson, J. D. Thompson, J. L. Smith, Z. Fisk and M. W. McElfresh. Kondo coherence in UBe₁₃: Magnetoresistance at high pressure. *Phys. Rev. Lett.* **63**, 2311-2314 (1989).
 - [20] F. J. Ohkawa. Magnetoresistance of Kondo lattices. *Phys. Rev. Lett.* **64**, 2300-2303 (1990).
 - [21] C. Chen, Z.-Z. Li, and W. Xu. Magneto-transport properties of heavy-fermion system. *J. Phys.: Condens. Matter* **5**, 95-104 (1993).
 - [22] A. Malinowski, M. F. Hundley, C. Capan, F. Ronning, R. Movshovich, N. O. Moreno, J. L. Sarrao, and J. D. Thompson. c -axis magnetotransport in CeCoIn₅. *Phys. Rev. B* **72**, 184506 (2005).
 - [23] S. Zaun, K. Grube, R. Schäfer, E. D. Bauer, J. D. Thompson, and H. v. Löhneysen. Towards the identification of a quantum critical line in the (p, B) phase diagram of CeCoIn₅ with thermal-expansion measurements. *Phys. Rev. Lett.* **106**, 087003 (2011).
 - [24] J. Paglione, T. A. Sayles, P. C. Ho, J. R. Jeffries, M. B. Maple. Incoherent non-Fermi-liquid scattering in a Kondo lattice. *Nature Physics* **3**, 703-706 (2007).
 - [25] P. Coleman, C. Pepin, Q. Si and R. Ramazashvili. How do Fermi liquids get heavy and die? *J. Phys.: Condens.*

- Matter* **13** R723-R738 (2001).
- [26] Dudy, J. D. Denlinger, L. Shu, M. Janoschek, J. W. Allen, and M.B. Maple. To be published.
 - [27] C. H. Booth, T. Durakiewicz, C. Capan, D. Hurt, A. D. Bianchi, J. J. Joyce, and Z. Fisk. Electronic structure and *f*-orbital occupancy in Yb-substituted CeCoIn₅. *Phys. Rev. B* **83**, 235117 (2011).
 - [28] V. S. Zapf *et al.*, *Phys. Rev. B* **65**, 014506 (2001).
 - [29] U. Schaufusse, V. Kataev, A. A. Zvyagin, B. Büchner, J. Sichelschmidt, J. Wykhoff, C. Krellner, C. Geibel, and F. Steglich. *Evolution of the Kondo State of YbRh₂Si₂ Probed by High-Field ESR*. *Phys. Rev. Lett.* **102**, 076405:1-4 (2009).
 - [30] P. Coleman, C. Pépin, Qimiao Si, and R. Ramazashvili. *How do Fermi liquids get heavy and die?*. arXiv:0105006 (2001).
 - [31] M. Dzero and Xinyi Huang. *"Correlated disorder in Kondo lattice."* *J. Phys: Cond. Mat.* **24**, 075603 (2012)